Catalysis Today 152 (2010) 70–77

Contents lists available at ScienceDirect

Catalysis Today

journal homepage: www.elsevier.com/locate/cattod

Effect of vanadia loading on the acidic, redox and catalytic properties of V_2O_5–TiO_2 and V_2O_5–TiO_2/SO_4^{2-} catalysts for partial oxidation of methanol

H. Zhao [a,b], S. Bennici [a], J. Cai [b], J. Shen [b], A. Auroux [a,*]

[a] Université Lyon 1, CNRS, UMR 5256, IRCELYON, Institut de recherches sur la catalyse et l'environnement de Lyon, 2 avenue Albert Einstein, F-69626 Villeurbanne, France
[b] Laboratory of Mesoscopic Chemistry, School of Chemistry and Chemical Engineering, Nanjing University, Nanjing 210093, China

ARTICLE INFO

Article history:
Available online 5 September 2009

Keywords:
V_2O_5–TiO_2
V_2O_5–TiO_2/SO_4^{2-}
Adsorption microcalorimetry
Acidic and redox properties
Methanol oxidation

ABSTRACT

V_2O_5/TiO_2 and V_2O_5/TiO_2–SO_4^{2-} catalysts with various vanadia loadings (5, 15 and 25 wt% V_2O_5) were prepared by successive incipient wetness impregnations and the effect of doping with SO_4^{2-} was studied. The catalysts were characterized by XRD, BET, XPS, Raman spectroscopy, redox cycles (TPR1/TPO/TPR2), ammonia adsorption microcalorimetry and tested in the selective oxidation of methanol to dimethoxymethane (DMM). The Raman spectra revealed the formation of crystalline V_2O_5 particles when the vanadia coverage was higher than 15 wt%. Redox cycles revealed that the monomeric vanadia species were easier to reduce but more difficult to oxidize than the polymeric and crystalline species. The supported vanadia species were found to be composed of stoichiometric V_2O_4 and V_2O_5, as shown by XPS. The ammonia adsorption microcalorimetric study evidenced acid sites with adsorption heats $Q_{diff} > 110$ kJ mol^{-1}, in amounts which increased upon the addition of SO_4^{2-} but decreased with increasing vanadia loading. Furthermore, the results of the methanol oxidation reaction suggest that the addition of SO_4^{2-} on highly dispersed supported vanadia catalysts promoted the catalytic activity.

1. Introduction

Supported vanadium systems, mainly on TiO_2 support, are among the most widely studied catalysts for the partial oxidation of methanol [1–6], which is known to proceed via dissociative chemisorption to form surface V-OCH_3 and support –OH intermediates [7,8]. Thus the nature and the surface area of the support as well as the structure of the vanadium species are all key factors in the formation of active surface species [9]. According to spectroscopic investigations, isolated monomeric vanadyl species, polymeric vanadia species and V_2O_5 crystallites may coexist on the titania support, their relative abundances being related to the vanadia content [10–13].

It is well known that the surface acidity exerts an important role in the partial oxidation of methanol, and it has been shown that the addition of SO_4^{2-} species to TiO_2 generates strong acidic sites at high temperature and can lead to high activity in the selective catalytic reduction (SCR) reaction [14]. Amiridis et al. [15] and Dunn et al. [16] have also reported that, on vanadia–titania catalysts, the gaseous SO_2 contained in the feed gas system could participate in the formation of surface sulfate species which strongly interact with vanadia and then improve the catalytic surface reactivity. Moreover, recent articles [17,18] show that the addition of the proper concentration of SO_4^{2-} to TiO_2 (anatase)-supported vanadium oxide can improve the catalytic activity in the selective oxidation of methanol to dimethoxymethane (DMM), which can undergo further steam reforming to produce hydrogen. Thus, it is very important to study the acidity of these solids in terms of the nature, amount, strength and strength distribution of their surface sites, from the fundamental and applicative points of view. Adsorption microcalorimetry of a basic probe molecule is a useful technique to describe, in detail, the quantitative and energetic features of the surface sites [19,20], and we have applied it to measure the acidity of the catalysts studied in this work.

Considering that most commercial titanias are sulfated to some extent due to the usual preparation procedure involving a sulfate, we investigated the influence of vanadia content in the presence of a very small amount of sulfate species (0.2–0.7 wt% S) in the reaction of selective oxidation of methanol to DMM. Moreover, in order to examine the role of sulfate species, sulfated vanadia–titania catalysts (1.1–1.8 wt% S) were prepared. Thus, this paper presents a study of the acidic and redox properties of V_2O_5–TiO_2 and V_2O_5–TiO_2/SO_4^{2-} catalysts with different amounts of vanadia and sulfate. The samples were fully characterized by XRD, BET, XPS and TPR/TPO. In addition, Raman spectroscopy was used to provide complementary information about the nature of the surface vanadium oxide species present in titania-supported vanadia

* Corresponding author. Fax: +33 472445399.
E-mail address: aline.auroux@ircelyon.univ-lyon1.fr (A. Auroux).

0920-5861/$ – see front matter © 2009 Elsevier B.V. All rights reserved.
doi:10.1016/j.cattod.2009.08.005

catalysts. A tentative correlation with the activity in partial oxidation of methanol was established.

2. Experimental

2.1. Catalyst preparation

Vanadium oxide systems with different V_2O_5 contents (denoted by VTi) supported on commercial TiO_2 (Millennium* G5, uncalcined) were prepared by incipient wetness impregnation, using ammonia vanadate (NH_4VO_3) as metal precursor and oxalic acid as complexing agent ($NH_4VO_3/C_2O_2H_2$ molar ratio = 1/2). After being kept at room temperature for 12 h to ensure their stabilization, the resulting solids were dried at 373 K overnight and then calcined in air at 673 K for 6 h. Pure TiO_2 catalyst, used as reference, was also calcined at 673 K in air for 6 h.

The sulfated vanadia–titania catalysts (denoted by VTiS) were prepared by incipient wetness impregnation of 1 g of above mentioned vanadia–titania catalysts with an aqueous solution containing the theoretical percentage of $(NH_4)_2SO_4$ to achieve 5 wt% SO_4^{2-} (1.7 wt% S). The resulting solids were then dried at 373 K overnight and calcined at 673 K in air for 6 h.

2.2. Catalyst characterization

Elemental analysis was performed using ICP atomic emission spectroscopy (ICP-AES) with a flame PerkinElmer M1100 spectrometer.

The surface areas, pore volumes and pore sizes were measured by nitrogen adsorption at 77 K on a Micromeritics 2010 apparatus after heat pretreatment under vacuum for 3 h at a temperature of 623 K.

The X-ray diffraction (XRD) measurements were carried out on a Bruker D5005 powder diffractometer scanning from 3° to 80° (2θ) at a rate of 0.02° s^{-1} using a Cu Kα radiation (λ = 0.15418 nm) source. The applied voltage and current were 50 kV and 35 mA, respectively.

The X-ray photoelectron spectra (XPS) were measured on a KRATOS AXIS Ultra DLD spectrometer equipped with a hemispherical electron analyzer and an Al anode (Al Kα = 1486.6 eV) powered at 150 W, a pass energy of 20 eV, and a hybrid lens mode. The detection area analyzed was 700 μm × 300 μm. Charge neutralization was required for all samples. The peaks were referenced to the C–(C, H) components of the C 1s band at 284.6 eV. Shirley background subtraction and peak fitting to theoretical Gaussian–Lorentzian functions were performed using an XPS processing program (Vision 2.2.6 KRATOS). The residual pressure in the spectrometer chamber was 5×10^{-9} mbar during data acquisition.

Raman spectroscopy measurements were performed using a LabRAM HR (Jobin Yvon) spectrometer. The excitation was provided by the 514.5 nm line of an Ar^+ ion laser (Spectra physics) employing a laser power of 100 μW. The laser beam was focused through microscope objective lenses (100×) down to a 1 μm spot on the sample.

Redox cycles (TPR1/TPO/TPR2), carried out in sequences consisting of a first temperature-programmed reduction (TPR) on the oxidized sample (TPR1), a temperature-programmed oxidation (TPO), and a second temperature-programmed reduction (TPR2), were performed using a TPD/R/O-1100 instrument (ThermoFisher). Prior to the TPR1 run, the fresh sample was treated in a stream of O_2/He (0.998% v/v, flowing at 20 mL min^{-1}), ramping the temperature at 10 K min^{-1} from RT to 623 K and maintaining it for 60 min, and then cooled to 313 K. The TPR1 measurement was carried out using H_2/Ar (4.98% v/v) as reducing gas mixture, flowing at 20 mL min^{-1}. The heating rate was 10 K min^{-1} from 313 K to 1073 K for VTi and VTiS systems and up to 1223 K for bulk V_2O_5. The TPO run was carried out on the reduced sample (after TPR1) cooled at 313 K in N_2 flow. After a purge with Ar (20 mL min^{-1}), the oxidizing gas mixture composed of O_2/He (0.998% v/v) flowed at 20 mL min^{-1} through the sample from 313 to 1073 K. The oxidized sample was further reduced during the TPR2 run, under the same experimental conditions as TPR1 described above, up to a final temperature of 1223 K for VTi and VTiS systems. The H_2 or O_2 consumption was detected by a thermal conductivity detector (TCD). The sample size used was adjusted in order to have around 69 μmol of V_2O_5 independently of the vanadia loading of the sample. This allowed us to maintain a K value of 100 s. The characteristic number, K, can be defined to facilitate the selection of appropriate operating parameters; a fixed K value between 60 and 140 s guarantees optimal conditions to obtain good TPR/TPO profiles [21,22]. The peak areas were calibrated with given H_2/Ar (4.98% v/v) and O_2/He (0.998% v/v) mixture injections for TPR and TPO, respectively.

The microcalorimetric studies of ammonia adsorption were performed at 423 K in a heat flow calorimeter (C80 from Setaram) linked to a conventional volumetric apparatus equipped with a Barocel capacitance manometer for pressure measurements. The ammonia used for measurements (Air Liquide, purity > 99.9%) was purified by successive freeze–pump–thaw cycles. About 100 mg of sample was pretreated in a quartz cell under evacuation overnight at 623 K. The differential heats of adsorption were measured as a function of coverage by repeatedly introducing small doses of ammonia gas onto the catalyst until an equilibrium pressure of about 66 Pa was reached. The sample was then outgassed for 30 min at the same temperature, and a second adsorption was performed at 423 K until an equilibrium pressure of about 27 Pa was attained in order to calculate the irreversibly chemisorbed amount of ammonia at this pressure.

2.3. Catalytic reaction

The oxidation of methanol was carried out in a fixed-bed microreactor made of glass with an inner diameter of 6 mm. The methanol was introduced into the reaction zone by bubbling O_2/N_2 (1/5) through a glass saturator filled with methanol (99.9%) maintained at 278 K. In each test, about 200 mg of catalyst was loaded, and the gas hourly space velocity (GHSV) was 11,400 mL g^{-1} h^{-1}. The feed composition was maintained as methanol:O_2:N_2 = 1:3:15 (v/v). The tail gas out of the reactor was analyzed by an on-line GC equipped with an FID detector and a TCD detector. The column used was PORAPAK N for the separation of methanol, DMM and other organic compounds. The gas lines were kept at 373 K to prevent condensation of the reactant and products. The reaction was carried out at atmospheric pressure.

3. Results and discussion

3.1. Structure properties

The X-ray diffraction patterns of the VTi and VTiS catalysts are shown in Fig. 1. The typical diffraction peaks characteristic of anatase TiO_2 were observed for all the catalysts. No crystalline vanadia phase appeared even for a V_2O_5 content close to 25 wt%, indicating that vanadium oxide was present in a highly dispersed manner. However, the presence of V_2O_5 crystallites with size less than 4 nm, which is beyond the detection capacity of the powder XRD technique, cannot be excluded. In addition, as shown in Fig. 1, the addition of SO_4^{2-} did not affect the dispersion of VTi catalysts.

The results of bulk (chemical analysis) and surface (XPS) analysis, the surface and bulk V/Ti ratios as well as the BET surface areas are listed in Table 1. TiO_2 possessed a high surface area of

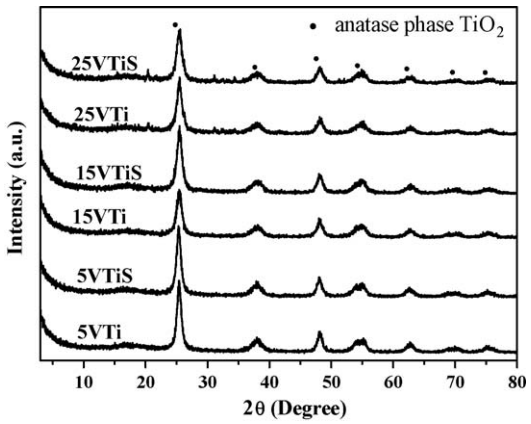

Fig. 1. X-ray diffraction (XRD) patterns of VTi and VTiS catalysts.

209 $m^2 g^{-1}$. Generally, in V_2O_5–TiO_2 systems the surface area continually decreases with increasing V_2O_5 content. In this work, the surface areas of the catalysts containing 5 and 15 wt% V_2O_5 were maintained around 200 $m^2 g^{-1}$ and then decreased to 165 $m^2 g^{-1}$ when the V_2O_5 content reached 25 wt%. In addition, the surface areas of the VTi catalysts also decreased upon addition of SO_4^{2-}. Similar pore volumes (0.26–0.38 $cm^3 g^{-1}$) and average pore sizes (5.7–6.4 nm) were obtained for all catalysts. As presented in Table 1, the commercial TiO_2 support in the supported vanadia catalyst was already sulfated with 0.2–0.7 wt% S, and the sulfur concentration in the VTiS systems slightly decreased from 1.76 wt% (5VTiS) to 1.11 wt% (25VTiS) with increasing vanadia loading. However, the surface and bulk V/Ti ratios were similar for all the catalysts, indicating that the vanadium was homogeneously distributed on the surface of TiO_2 support.

Table 2 presents the binding energies (BE) of V $2p_{3/2}$, O 1s, Ti $2p_{3/2}$ and S $2p_{1/2}$ lines and the relative components from the decomposition of V $2p_{3/2}$ and O 1s lines. The binding energy references [23,24] of the V $2p_{3/2}$ line for V_2O_5 and V_2O_4 are around 517.5 and 516.4 eV, respectively. As seen in Table 2, all the catalysts exhibited about 20% V^{4+} species, except the 5VTi and 5VTiS samples which were more reduced, presenting a contribution of ~50% V^{4+}. This difference observed at low vanadia loading indicates that a high dispersion of vanadium oxide could favor the reduction of V(V) to V(IV) upon exposure to X-radiation under ultra-high vacuum operating conditions. The BE position of the Ti $3p_{3/2}$ line was around 459.0 ± 1 eV and maintained for all the catalysts, suggesting the presence of Ti^{4+} of TiO_2 [25]. The XPS spectra of the S 2p line displayed the same band centered at 169.0 eV, which is typical of sulfur in the S^{6+} oxidation state and in the form of bidentate sulfate (SO_4^{2-}) species on the surface of TiO_2 [26,27].

In a previous paper [28] we have already reported that the O 1s spectra can be decomposed into three peaks to gain information about the O 1s components, which are the lattice oxygen of the TiO_2 + V_2O_5 oxides, the bridged oxygen of surface hydroxyl groups (Ti–OH) and the oxygen of sulfates (SO_4^{2-}) respectively. We obtained the same results in this work for all VTi and VTiS samples.

The surface structure of vanadia and titania species on the VTiS catalysts was examined by Raman spectroscopy, from 1600 to 200 cm^{-1}, as shown in Fig. 2. Previous studies by Wachs et al. [10–13,29,30] have already shown that, depending on the vanadia loading, two types of surface vanadia species and microcrystalline phase V_2O_5 particles can be present on the surface of V_2O_5–TiO_2 catalysts. Under hydrated conditions and at low surface coverage a broad Raman band at ~940 cm^{-1} is present, corresponding to the distorted tetrahedral vanadia species in polymeric metavanadate compounds. This band quickly shifts to ~994 cm^{-1} as the vanadia loading is increased, which is due to microcrystalline V_2O_5 [13,29]. The Raman spectra of the catalysts prepared for this work were in agreement with the observations reported in the literature.

For the present catalysts, broad Raman bands at 947 and 807 cm^{-1} assigned to polymerized vanadia species were detected for the submonolayer coverage [10] corresponding to approximately 5 wt% vanadia, regardless of whether SO_4^{2-} was added.

Table 1
Chemical analysis, X-ray photoelectronic spectroscopy analysis, V/Ti atomic ratios for surface and bulk composition and BET surface area of the samples.

Sample	S_{BET} ($m^2 g^{-1}$)	C.A. (wt%)			XPS (wt%)			V/Ti (surface atomic ratio)	V/Ti (bulk atomic ratio)
		V	Ti	S	V	Ti	S		
5VTi	197	2.82	50.42	0.62	4.45	48.43	0.53	0.09	0.06
5VTiS	174	2.74	50.13	1.76	3.40	46.41	3.33	0.07	0.05
15VTi	206	7.73	48.48	0.18	8.34	45.71	0.65	0.17	0.16
15VTiS	178	8.05	47.02	1.41	7.75	43.78	2.50	0.17	0.15
25VTi	165	14.45	40.77	0.68	18.98	36.32	Traces	0.5	0.4
25VTiS	134	13.82	38.87	1.11	14.69	36.75	1.84	0.38	0.4
TiO_2	209	–	–	<0.2	–	–	<0.2	–	–

Table 2
Binding energies and concentration (in atomic %) of the different oxygen (TiO_2 + V_2O_5, –OH, and –SO_4^{2-}) and vanadia species present on the surface of VTi and VTiS catalysts.

Sample	Binding energy (ev)						
	V $2p_{3/2}$		O 1s			Ti $2p_{3/2}$	S $2p_{1/2}$
	V_2O_4	V_2O_5	TiO_2 and V_2O_5	–OH	SO_4^{2-}		
5VTi	516.0 (53%)	17.0 (47%)	29.8 (81%)	30.9 (12%)	531.9 (7%)	458.6	168.5
5VTiS	516.1 (52%)	17.1 (47%)	530.0 (72%)	531.1 (11%)	531.9 (17%)	458.8	168.7
15VTi	516.4 (21%)	517.7 (79%)	530.3 (82%)	531.0 (9%)	532.0 (9%)	459.1	168.9
15VTiS	516.4 (19%)	517.6 (81%)	530.4 (74%)	531.1 (9%)	532.1 (17%)	459.0	168.8
25VTi	516.2 (17%)	517.4 (83%)	530.2 (87%)	531.3 (13%)	–	459.0	169.0
25VTiS	516.3 (16%)	517.5 (84%)	530.1 (77%)	531.3 (12%)	531.9 (11%)	459.0	169.0

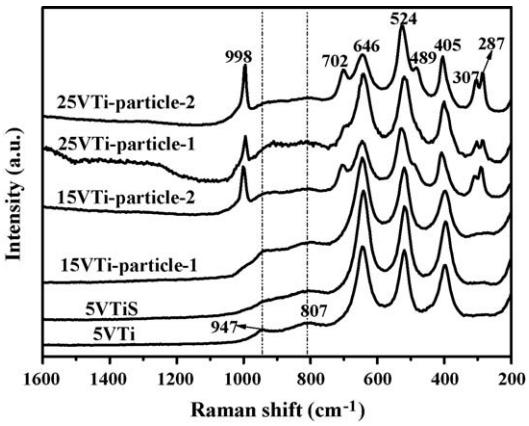

Fig. 2. Raman spectra of VTi and VTiS catalysts.

Upon increasing the vanadia loading up to 15 wt%, the catalyst became heterogeneous, and consequently both types of particles were analyzed. 15VTi-particle-1 exhibited the Raman bands due to polymeric vanadate species, similar to those of sample 5VTi, while 15VTi-particle-2 gave rise to strong Raman bands typical of crystalline V_2O_5 around 998, 702, 524, 489, 425, 307 and 287 cm^{-1}. The catalyst with 25 wt% vanadia content is also rather heterogeneous, as shown by 25VTi-particle-1 and 25VTi-particle-2, but the major Raman band at 998 cm^{-1} due to crystalline V_2O_5 could be detected on both types of particles.

3.2. Redox cycles with temperature-programmed reduction and oxidation

The reversibility in a redox cycle of the VO_x species of the studied VTi and VTiS catalysts was investigated by TPR and oxidation analysis (TPR1/TPO/TPR2 cycle). Table 3 summarizes the most important results, in terms of maximum temperatures (T_{m1} and T_{m2}) of the reduction and oxidation peaks and of the integrated H_2 and O_2 consumptions. Fig. 3 shows the reduction and oxidation profiles of all the studied catalysts.

Table 3
Redox behavior of the VTi and VTiS catalysts from TPR/TPO experiments.

Sample	Experiment	The maximum temperatures of peaks		Reduction *or* oxidation
		Peak 1 (T_{m1})	Peak 2 (T_{m2})	(μmol H_2 g_v^{-1}) *or* (μmol O_2 g_v^{-1})
5VTi	TPR1	749	976	29,043
	TPO	829	–	9,468
	TPR2	873	n.d.[a]	20,248
5VTiS	TPR1	813	993	48,759
	TPO	838	–	8,905
	TPR2	853	n.d.[a]	19,964
15VTi	TPR1	730, 774	944	28,616
	TPO	777	–	10,065
	TPR2	916	n.d.[a]	20,272
15VTiS	TPR1	753, 784	945	32,932
	TPO	775	878	10,075
	TPR2	1015	n.d.[a]	21,193
25VTi	TPR1	749, 797	928	24,394
	TPO	775	924	9,433
	TPR2	931	1084	19,702
25VTiS	TPR1	752, 802	930	27,236
	TPO	773	921	8,813
	TPR2	929	n.d.[a]	21,845
Pure V_2O_5	TPR1	938, 974	1110, 1195	22,096
	TPO	779	935	10,379
	TPR2	978, 1015	n.d.[a]	23,513

[a] Not determined.

3.2.1. Temperature-programmed reduction in H_2

When reducing bulk V_2O_5 in the temperature range from RT up to 1223 K, four peaks were observed, located at 938, 974, 1110 and 1195 K, respectively. The first peak should be assigned to the formation of V_6O_{13}, the second to VO_2, and with the completion of hydrogen consumption V_2O_3 is reached [31]. For the VTi and VTiS systems, conventional TPR runs were carried out up to 1073 K only to study the reducibility of the vanadia species. More than one reduction peak was observed, indicating the presence of several types of oxygen-containing vanadium species on the TiO_2 surface. In addition, considering that different vanadia species such as monomeric, polymeric and crystalline VO_x species may coexist at the surface of the studied catalysts, the peaks do not necessarily represent different steps of reduction of the same species but should rather be considered to result from a superposition of reduction steps of several different species [29]. Referring to the literature [32], the maximum temperature of reduction peaks (T_{m1}) in the low-temperature region (<900 K) indicates the presence of monomeric VO_x species ($T_{m1} \leq 770$ K) and polymeric VO_x species ($T_{m2} = 774$–813 K) in the VTi and VTiS systems (Table 3).

From a comparison of the TPR profiles of the VTi samples, T_{m1} of reduction peaks was found to be shifted to higher values with increasing V_2O_5 content, indicating that more polymeric vanadia species might be formed, as confirmed by Raman spectroscopy measurements. Additionally, the addition of SO_4^{2-} might inhibit the reduction of vanadia, since the reduction peak maxima shifted to higher temperatures for samples with low V_2O_5 content, possibly due to an increased proportion of polymeric vanadia species upon re-calcination, or due to the formation of the sulfate species "crowding" the vanadyl species together and leading to more polymerization [15].

For example, an increase of 60 K was observed for the T_{m1} value of sample 5VTiS compared to sample 5VTi (5VTi: $T_{m1} = 749$ K; 5VTiS: $T_{m1} = 813$ K). When the V_2O_5 content was increased to 15 wt%, this peak ($T_{m1} = 784$ K) acquired a shoulder at lower temperature (753 K), indicating that insoluble vanadium species became heterogeneous, which was consistent with the Raman spectra showing that sample 15VTi contained both polymeric VO_x and microcrystalline V_2O_5 particles. When the V_2O_5 content reached 25 wt%, a similar TPR behavior was detected with sample 25VTi (see Table 3).

Furthermore, considering the rather different amounts of reducible VO_x species in VTi and VTiS systems, the H_2 consumption has been expressed as μmol H_2 per gram of vanadium (μmol g_v^{-1}). Obviously, the H_2 consumption continually decreased with increasing V_2O_5 content, possibly due to the formation of highly polymeric VO_x species. However, the H_2 consumption increased with the introduction of SO_4^{2-}, thus indicating the reduction of SO_4^{2-} ions [33].

3.2.2. Temperature-programmed oxidation after TPR with O_2

The reoxidation behavior of the catalysts starting from the V^{3+} oxidation state obtained after TPR1 was analyzed by TPO. The TPO profiles are shown in Fig. 3(a) and (b) TPO. The TPO profiles of bulk V_2O_5 exhibit two separate peaks ($T_{m1} = 779$ K and $T_{m2} = 935$ K). Hence, oxidation occurs at lower temperature than reduction with hydrogen. The TPO profiles resemble more or less the TPR profiles viewed from higher to lower temperature. This suggests that the transitions observed in the TPR experiments are reversed in the TPO experiments. Thus, for bulk V_2O_5, the peak at 779 K corresponds to the transition of V_2O_3 to VO_2, and the second peak at 935 K to the formation of V_2O_5. For VTi and VTiS systems,

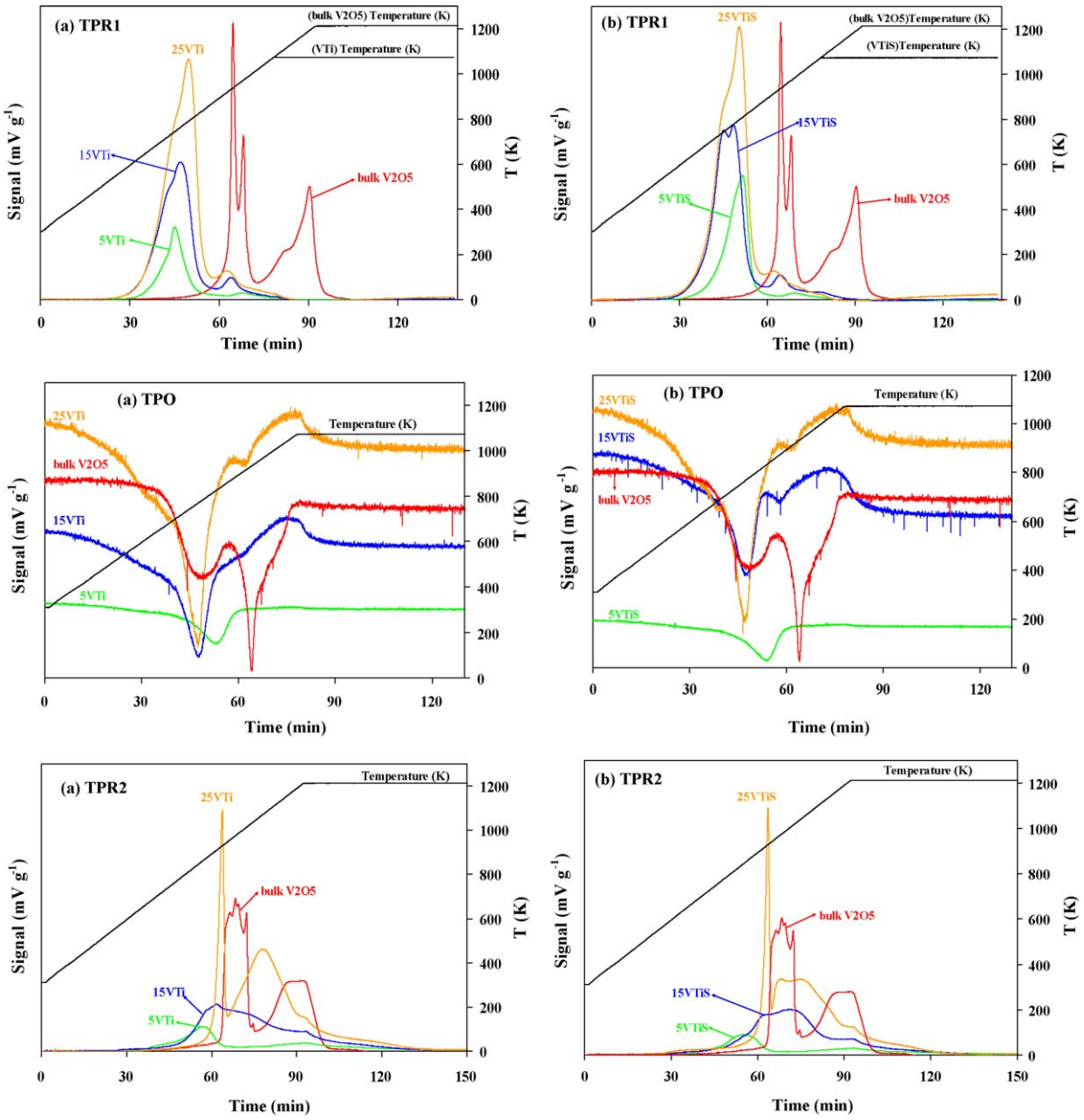

Fig. 3. Redox cycles of (a) VTi catalysts, (b) VTiS catalysts and bulk V_2O_5. Profiles of reduction (TPR1, TPR2) and oxidation (TPO) as a function of temperature and time (10 K min^{-1}) (bulk V_2O_5, red; 5VTi and 5VTiS, green; 15VTi and 15VTiS, blue; 25VTi and 25VTiS, orange). All spectra were magnified (5×) except bulk V_2O_5. (For interpretation of the references to colour in this figure legend, the reader is referred to the web version of the article.)

Table 4
Ammonia adsorption data from microcalorimetry measurements at 423 K.

Sample	V_{tot}[a] (27 Pa) (μmol g^{-1})	V_{tot}[a] (27 Pa) (μmol m^{-2})	V_{irr}[b] (μmol g^{-1})	V_{irr}[b] (μmol m^{-2})	Q_{init}[c] (kJ mol^{-1})
5VTi	498	2.5	291	1.5	194
5VTiS	486	2.8	316	1.8	219
15VTi	483	2.3	275	1.3	210
15VTiS	514	2.9	335	1.9	231
25VTi	425	2.6	213	1.3	220
25VTiS	406	3.0	243	1.8	145
TiO_2	517	2.5	279	1.3	210

[a] Total amount of NH_3 retained as determined at 27 Pa of equilibrium pressure.
[b] "Irreversible" amount of NH_3 retained as determined from the difference between the amounts adsorbed in the first and second adsorptions at 27 Pa.
[c] Heat evolved from the first NH_3 dose.

Table 5
Catalytic activities of the VTi and VTiS catalysts in the methanol oxidation reaction.

Sample	Temp. (K)	Con. of methanol (%)	Selectivity (%)				
			DMM	FA	MF	DME	CO_x
5VTi	403	6	88	6	6	0	0
	413	9	74	8	17	0	0
	423	12	59	12	28	0	0
	433	21	30	13	57	0	0
	453	41	9	20	59	1	11
5VTiS	403	12	87	0	0	13	0
	413	19	85	0	0	15	0
	423	28	77	3	1	19	0
	433	32	47	10	32	12	0
	453	71	6	16	19	23	36
15VTi	403	22	90	3	7	0	0
	413	37	59	6	34	1	0
	423	51	28	12	58	1	1
	433	84	0	6	13	0	81
15VTiS	403	22	94	1	2	2	0
	413	36	84	2	11	3	0
	423	52	53	5	39	3	0
	433	86	1	7	12	2	77
25VTi	403	31	93	2	4	0	0
	413	49	74	7	19	1	0
	423	67	24	17	58	1	0
	433	92	0	2	35	2	61
25VTiS	403	25	95	2	1	2	0
	413	36	85	7	7	1	0
	423	58	54	13	31	2	0
	433	92	0	1	37	5	56

DMM: dimethoxymethane, FA: formaldehyde, MF: methyl formate, DME: dimethyl ether, CO_x: CO_2 (or CO).

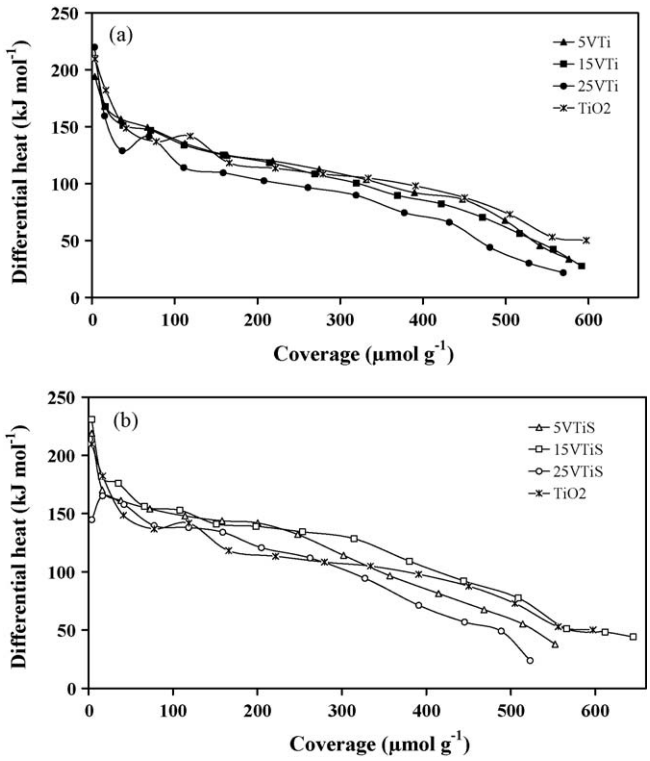

Fig. 4. Differential heat versus coverage (in μmol g^{-1} of catalyst) for NH_3 adsorption at 423 K over (a) VTi and (b) VTiS catalysts.

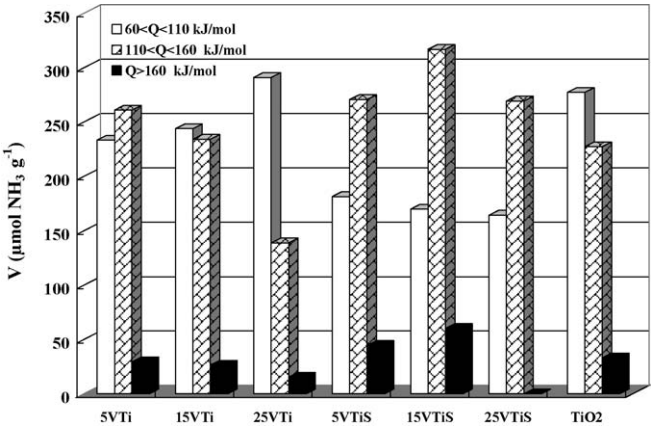

Fig. 5. Acidity spectra of the VTi and VTiS catalysts.

the same transitions that were observed in TPR are also seen in TPO, being inversely related. Compared to bulk V_2O_5, the supported vanadia catalysts (VTi and VTiS) are not only easier to reduce but also easier to reoxidize, indicating that the support promotes both reduction and reoxidation. From a comparison of TPR1 and TPO profiles, it appears that the polymeric or crystalline vanadia species present on the TiO_2 support are the easiest to reoxidize but most difficult to reduce, whereas highly dispersed vanadia species present on TiO_2 are the easiest to reduce but the most difficult to reoxidize. This is in agreement with the results obtained by Majunke and Baerns [34].

3.2.3. Temperature-programmed reduction after TPO with H_2

A second reduction analysis (TPR2) was performed on the samples freshly reoxidized by TPO. Fig. 3(a) and (b) TPR2 comparatively present the collected reduction profiles. As shown in this figure, part of the vanadia species were not reduced at the temperature of 1223 K, and the remaining part necessitated a much higher temperature to be reduced, which made it difficult to reach the maximum of the reduction peak and the stoichiometric consumption of hydrogen. In all cases, the positions and shapes of the peaks of the TPR2 profiles were different from those of TPR1; the TPR2 profiles showed a shift toward higher temperatures than TPR1. The lack of overlap between TPR1 and TPR2 suggested a mobility of the vanadia species leading to more aggregated vanadia phase [35]. The newly created vanadia species were more crystalline, especially for the sample with 25 wt% V_2O_5 which presented the highest reduction temperatures.

3.3. Acidity properties

The acidity of the catalysts was determined by ammonia adsorption microcalorimetry [20]. Table 4 presents the initial heats of adsorption (denoted by Q_{init}) and the amount of ammonia adsorbed under an equilibrium pressure of 27 Pa. Fig. 4 displays the differential heats of ammonia adsorption as a function of coverage for the VTi and VTiS catalysts and pure TiO_2 support, while Fig. 5 shows the acid site strength distribution of the catalysts which gives the number of sites of a given strength.

The initial heat of ammonia adsorption on TiO_2 was found to be about 210 kJ mol^{-1}, suggesting that the TiO_2 support used in this work is strongly acidic. The addition of V_2O_5 did not change significantly the initial heat, while the addition of SO_4^{2-} slightly increased the initial heat except for the 25VTiS sample. Additionally, the amount of irreversibly absorbed ammonia (V_{irr}), corresponding to strong chemisorption, decreased with increasing V_2O_5 content, but the strong acid site densities became similar when V_{irr} was expressed per unit surface area, which reveals that the decrease of the number of acid sites can be attributed to the

decrease of surface area. Nevertheless, the number and the density of strong acid sites (see V_{irr}) increased upon the addition of SO_4^{2-}.

We have shown in previous studies [28] on sulfated vanadia–titania prepared by sol–gel that the first doses of ammonia were fully adsorbed with very low heats evolved, thus inducing very low initial differential heats of adsorption. This observation was explained by a combination of both an endothermic effect such as NH_3 dissociation [36] or the formation of ammonium sulfite [37] and the exothermic adsorption; however, such an effect was not observed in the present study, or only to a very low extent on sample 25 VTiS. Moreover, the heat of NH_3 adsorption gradually decreased with NH_3 coverage for all the studied catalysts, suggesting a heterogeneous strength distribution of these catalysts, as shown in Fig. 4.

Fig. 5 shows the acid site strength distributions of all the catalysts. For the VTi samples, the populations of strong acid sites ($Q_{diff} > 160$ kJ mol^{-1}) and medium acid sites ($110 < Q_{diff} < 160$ kJ mol^{-1}) decreased with increasing amount of V_2O_5, while the amount of weak acid sites with $60 < Q_{diff} < 110$ kJ mol^{-1} increased. For the VTiS samples, it is clear that the strong and medium acid sites increased upon the addition of SO_4^{2-} even if the low initial heats of adsorption made it difficult to calculate the number of strong acid sites for sample 25VTiS.

3.4. Selective oxidation of methanol

The selective oxidation of methanol to dimethoxymethane (DMM) may involve two steps: (1) oxidation of methanol to formaldehyde on redox sites and (2) condensation of formaldehyde produced with additional methanol to form DMM on acidic sites. Thus, bifunctional catalysts with redox and acidic characters are required for the reaction. In addition, the relative strengths of surface acidity and redox ability of a catalyst may be important in determining reaction pathways as well as selectivity to DMM.

In this work, the conversion of methanol increased with increasing V_2O_5 content, due to enhanced redox properties. This behavior supported the results of the TPR1 measurements, in which the H_2 consumption (expressed as μmol H_2 per gram of catalyst and not per g of V) increased with the vanadia loading. Meanwhile, the selectivity to DMM increased slightly upon the addition of SO_4^{2-} due to the enhanced acidity (see Table 5). Nevertheless, samples 15VTiS and 25VTiS possessed similar catalytic behaviors even as the vanadia content increased from 15 to 25 wt%. Many researchers claim that amorphous monomeric VO_x species with terminal V=O bonds are the most active species for reactant adsorption and C–H bond breaking, particularly when compared to crystalline V_2O_5 [38–41]. As evidenced by Raman spectroscopy, crystalline V_2O_5 species are present on sample 15VTi, and even more crystalline V_2O_5 particles were detected for sample 25VTi. The formation of crystalline V_2O_5 species with increasing vanadia loading would also be applicable to the polymeric vanadia species in the VTiS systems, as evidenced by TPR measurements.

Among all the VTi and VTiS catalysts, sample 25VTiS showed the highest yield at the reaction temperature of 423 K, with 58% methanol conversion and 54% DMM selectivity. Fu and Shen [17] have already reported positive effects upon the addition of different sulfates to the V_2O_5/TiO_2 system for the selective oxidation of methanol to DMM. They mention good results over $Ti(SO_4)_2$-modified V_2O_5/TiO_2 catalysts ($S_{BET} = 82$ m^2 g^{-1}; V_2O_5% = 10 wt%; S% = 0.2 wt%) with DMM selectivities of 89–92% for 48–60% methanol conversions. It seems that the enhanced DMM selectivity is strongly affected not simply by the addition of SO_4^{2-}, but also by the nature of the sulfate-carrier–vanadia interaction, the amount of exposed carrier surface, the vanadia loading, and the catalyst surface area. In addition, when sulfated species ($(NH_4)_2SO_4$) were added to the VTi system, the conversion of methanol obviously increased for sample 5VTiS and the selectivity to DME (created on strong acid sites) too, which suggests that the addition of SO_4^{2-} on a "monolayer-type" vanadia–titania catalyst easily improves both the redox (confirmed by TPR experiments) and surface acidity properties. Thus, these results indicate that monomeric and polymeric vanadia, as opposed to crystalline V_2O_5, are the most reactive species in methanol oxidation, a model reaction for V_2O_5/TiO_2 catalysts.

4. Conclusion

A series of V_2O_5–TiO_2 (VTi) catalysts were prepared by incipient wetness impregnation and modified with SO_4^{2-} species. Raman spectroscopy suggested that microcrystalline V_2O_5 particles started to be formed for sample 15VTi. Moreover, the Raman spectra also suggested that the samples with higher vanadia loadings were not homogeneous. XPS showed that titanium and sulfur were present in their fully oxidized states for all the VTi and VTiS catalysts, while the state of vanadium was composed of stoichiometric pentavalent and tetravalent V. The maxima of the reduction peaks in TPR1 profiles indicated the presence of isolated monomeric vanadia species ($T_{m1} \leq 770$ K) and polymeric vanadia species ($T_{m1} = 774$–813 K) on the support surface. The monomeric species are more easily reduced but more difficult to oxidize than the polymeric and crystalline species. The ammonia adsorption calorimetry study showed that the number of acid sites with $Q_{diff} > 110$ kJ mol^{-1} was obviously increased upon the addition of SO_4^{2-}. The best catalytic behavior in this work was obtained on sample 25VTiS with, 58% DMM selectivity for 58% methanol conversion at 423 K. Consequently, the acidic and redox properties were related with the vanadia content and the addition of sulfate species, which finally affected the catalytic behavior of the methanol oxidation to dimethoxymethane.

Acknowledgements

The authors are thankful to the scientific services of IRCELYON, in particular to Laurence Massin for providing XPS measurements and to Marlène Daniel for providing Raman spectroscopy measurements.

Hongying Zhao gratefully acknowledges the China Scholarship Council for the financial support of her PhD grant.

Financial supports from NSFC (20673055) and MSTC (2005CB221400 and 2004DFB02900) are acknowledged.

References

[1] P. Forzatti, E. Tronconi, G. Busca, P. Tittarelli, Catal. Today 1 (1987) 209–218.
[2] F. Roozeboom, P.D. Cordingley, P.J. Gellings, J. Catal. 68 (1981) 464–472.
[3] A. Baiker, D. Monti, J. Catal. 91 (1985) 361–365.
[4] G.C. Bond, S.F. Tahir, Appl. Catal. 71 (1991) 1–31.
[5] P. Forzatti, E. Tronconi, A.S. Elmi, G. Busca, Appl. Catal. A: Gen. 157 (1997) 387–408.
[6] Q. Wang, R.J. Madix, Surf. Sci. 496 (2002) 51–63.
[7] A. Khodakov, B. Olthof, A.T. Bell, E. Iglesia, J. Catal. 181 (1999) 205–216.
[8] G. Busca, J. Mol. Catal. 50 (1989) 241–249.
[9] M.A. Banares, M.V. Martinez-Huerta, X. Gao, J.L.G. Fierro, I.E. Wachs, Catal. Today 61 (2000) 295–301.
[10] I.E. Wachs, Catal. Today 27 (1996) 437–455.
[11] I.E. Wachs, B.M. Weckhuysen, Appl. Catal. A: Gen. 157 (1997) 67–90.
[12] G. Deo, I.E. Wachs, J. Haber, Crit. Rev. Surf. Chem. 4 (1994) 141–187.
[13] I.E. Wachs, G. Deo, B.M. Weckhuysen, A. Andreini, M.A. Vuurman, M. De Boer, M.D. Amiridis, J. Catal. 161 (1996) 211–221.
[14] S.M. Jung, P. Grange, Catal. Today 59 (2000) 305–312.
[15] M.D. Amiridis, I.E. Wachs, G.D. Deo, J.M. Jehng, D.S. Kim, J. Catal. 161 (1996) 247–253.
[16] J.P. Dunn, H.G. Stenger Jr., I.E. Wachs, J. Catal. 181 (1999) 233–243.
[17] Y. Fu, J. Shen, Chem. Commun. 21 (2007) 2172–2174.
[18] S. Royer, X. Sécordel, M. Brandhorst, F. Dumeignil, S. Cristol, C. Dujardin, M. Capron, E. Payen, J.-L. Dubois, Chem. Commun. 7 (2008) 865–867.

[19] N. Cardona-Martinez, J.A. Dumesic, Adv. Catal. 38 (1992) 149–244.
[20] A. Auroux, Top. Catal. 4 (1997) 71–89.
[21] P. Malet, A. Caballero, J. Chem. Soc., Faraday Trans. I 84 (1988) 2369–2375.
[22] D.A.M. Monti, A. Baiker, J. Catal. 83 (1983) 323–335.
[23] S.L.T. Andersson, J. Chem. Soc., Faraday Trans. I 75 (1979) 1356–1370.
[24] J.A. Odriozola, J. Soria, G.A. Somorjai, H. Heinemann, J.F. Garcia de la Banda, M. Lopez Granados, J.C. Conesa, J. Phys. Chem. 95 (1991) 240–246.
[25] J. Keränen, C. Guimon, E. Iiskola, A. Auroux, L. Niinistö, Catal. Today 78 (2003) 149–157.
[26] M.H. Kim, I.-S. Nam, Y.G. Kim, J. Catal. 179 (1998) 350–360.
[27] D. Fraenkel, Ind. Eng. Chem. Res. 36 (1997) 52–59.
[28] H. Zhao, S. Bennici, J. Shen, A. Auroux, Appl. Catal. A: Gen. 356 (2009) 121–128.
[29] G.T. Went, L.-J. Leu, A.T. Bell, J. Catal. 134 (1992) 479–491.
[30] I.E. Wachs, J. Catal. 124 (1990) 570–573.
[31] S. Besselmann, C. Freitag, O. Hinrichsen, M. Muhler, Phys. Chem. Chem. Phys. 3 (2001) 4633–4638.
[32] G.Y. Popova, T.V. Andrushkevich, E.V. Semionova, Y.A. Chesalov, L.S. Dovlitova, V.A. Rogov, V.N. Parmon, J. Mol. Catal. A: Chem. 283 (2008) 146–152.
[33] B.Q. Xu, W.M.H. Sachtler, J. Catal. 167 (1997) 224–233.
[34] F. Majunke, M. Baerns, Catal. Today 20 (1994) 53–60.
[35] S. Bennici, A. Auroux, in: D. Jackson, J. Hargreaves (Eds.), Metal Oxide Catalysis, vol. 1, Wiley-VCH, 2009, pp. 391–436.
[36] A. Desmartin-Chomel, J.L. Flores, A. Bourane, J.M. Clacens, F. Figueras, G. Delahay, A. Giroir Fendler, C. Lehaut-Burnouf, J. Phys. Chem. B 110 (2006) 858–863.
[37] A. Gervasini, J. Fenyvesi, A. Auroux, Langmuir 12 (1996) 5356–5364.
[38] J.C. Vedrine (Ed.), EUROCAT oxide Catal. Today 20 (1994).
[39] G.C. Bond, J. Chem. Technol. Biotechnol. 68 (1997) 6–13.
[40] C.R. Dias, M.F. Portela, G.C. Bond, J. Catal. 157 (1995) 344–352.
[41] G. Centi, Appl. Catal. A: Gen. 147 (1996) 267–298.